Big Jump of Record Warm Global Mean Surface Temperature in 2014-2016 Related to Unusually Large Oceanic Heat Releases

Jianjun Yin[1,2,3*], Jonathan Overpeck[4], Cheryl Peyser[1] and Ronald Stouffer[1]

1. Department of Geosciences, University of Arizona
2. Program in Atmospheric and Oceanic Sciences, Princeton University
3. GFDL/NOAA
4. School for Environment and Sustainability, University of Michigan

Key Points:

- A 0.24°C jump of record warm global mean surface temperature over the past three consecutive years (2014-2016) was highly unusual
- It was a result of an El Niño that released unusually large amounts of ocean heat previously accumulated in the western tropical Pacific
- Large record-breaking events of global surface temperature are projected to increase in the future unless greenhouse-gas forcing is reduced

* Corresponding author address: Dr. Jianjun Yin, Department of Geosciences, University of Arizona; Email: yin@email.arizona.edu; Phone: (520) 626-7453

Abstract

A 0.24°C jump of record warm global mean surface temperature (GMST) over the past three consecutive record-breaking years (2014-2016) was highly unusual and largely a consequence of an El Niño that released unusually large amounts of ocean heat from the subsurface layer of the northwestern tropical Pacific (NWP). This heat had built up since the 1990s mainly due to greenhouse-gas (GHG) forcing and possible remote oceanic effects. Model simulations and projections suggest that the fundamental cause, and robust predictor of large record-breaking events of GMST in the 21st century is GHG forcing rather than internal climate variability alone. Such events will increase in frequency, magnitude and duration, as well as impact, in the future unless GHG forcing is reduced.

1. Introduction

The annual mean GMST broke the previous records three years in a row during 2014-2016 and by a large margin. The magnitude and duration of this record-breaking event were highly unusual [*Mann et al.*, 2017] and exceeded previous events associated with strong El Niño. As a consequence, global warming has passed the 1°C milestone relative to the pre-industrial period (1851-1880), with some monthly GMST values in 2015 and 2016 even close to the 1.5°C threshold. This jump of record warm GMST also represents a sizable fraction of the 2°C stabilization goal set by the 2015 Paris Agreement [*Paris Agreements*, 2015] to avoid dangerous climate change. The record high monthly and annual mean GMST in 2015 and 2016 were coincident with outbreaks of extreme weather worldwide [*Herring et al.*, 2016; *Herring et al.*, 2018], extensive melting of polar ice [*Nicolas et al.*, 2017; *Simpkins*, 2017], as well as the third ever global coral bleaching event [*NOAA*, 2015]. Given these significant impacts, it is extremely important and timely to understand the mechanism for this rapid warming and provide perspectives for future large record-breaking events of GMST. Here we examine various observational data and the simulations and projections by 40 climate models to address these issues.

2. Data and Models

Table 1 summarizes the observational datasets used in the present study. Six datasets are available for GMST including HadCRUT4 [*Morice et al.*, 2012], GISTEMP [*Hansen et al.*, 2010], NOAAGlobalTemp [*Vose et al.*, 2012], JMA [*Ishihara*, 2006], Berkeley [*Rohde et al.*, 2013] and Cowtan&Way [*Cowtan and Way*, 2014]. The detailed data descriptions and uncertainty quantification can be found in the references (Figure S1). All six GMST datasets were downloaded as of March 7, 2017.

As closely related fields, we use three datasets for ocean heat content (OHC) and temperatures including Levitus [*Levitus et al.*, 2012], Ishii [*Ishii and Kimoto*, 2009] and Argo [*Roemmich and Gilson*, 2009] (Table 1). The OHC anomalies are relative to the WOA09, 1981-2010 and 2004-2015 climatology in the three datasets, respectively. The values are integrated in the upper 700 m and across each grid box. It should be noted that the three datasets are not independent. The Argo coverage is usually not considered adequate until 2005.

We choose two tide gauge data in the NWP with relatively long and complete records (Table 1) [*Holgate et al.*, 2013]. The relative sea level data at Kwajalein (167.74°E, 8.73°N) and Guam (144.65°E, 13.44°N) span from 1950-2015 and 1948-2016, respectively. For satellite altimetry data, we use the Archiving, Validation, and Interpretation of Satellite Oceanographic data (AVISO) (Table 1) [*Ducet et al.*, 2000]. The data show dynamic sea level (i.e., departure of sea surface height from the geoid) at an eddy-resolving scale and over a global domain. We find that the tide gauge and altimetry data are highly correlated at Kwajalein and Guam during 1993-2016 (r=0.98), and show similar interannual changes and decadal/interdecadal trends (Figure S2). The long-term global mean sea level reconstruction is from *Church and White* [2011].

The Multivariate ENSO Index (MEI) is a comprehensive index for quantifying ENSO strength (Table 1) [*Wolter and Timlin*, 2011]. According to the MEI time series (Figure S3), the 2015/2016 El Niño was strong but not as strong as the 1982/1983 and 1997/1998 El Niño. Although there were signs of El Niño development in 2014 [*Hu and Fedorov*, 2016], 2015 was the real onset of the recent strong El Niño. As another widely used index, Niño3.4 confirms the strong El Niño in 1982/1983, 1997/1998 and 2015/2016 (Figure S3) [*Rayner et al.*, 2003]. To identify decadal and longer time scale variability in the Pacific, we apply a 9-year low-pass filter to the annual mean index of the Pacific Decadal Oscillation (PDO) (Figure S4). We quantify the

contribution of PDO to the ocean heat accumulation and sea level rise in the western tropical Pacific (WP) during 1993-2012. The use of the Interdecadal Pacific Oscillation (IPO) index gives similar results.

In terms of modeling data, we use 40 CMIP5 models and their piControl and 20th century simulations, as well as 21st century projections under four RCP emission scenarios (Table S1) [*Flato et al.*, 2013; *Taylor et al.*, 2012]. Based on the 200-year piControl simulations, the CMIP5 models show a range of internal variability of GMST (as the standard deviation of the annual time series) from 0.06°-0.16°C, with an ensemble mean of 0.11°C (Table S2). For observational estimates, we apply the Ensemble Empirical Mode Decomposition method [*Wu et al.*, 2011] to remove the nonlinear secular trend from the observed GMST time series (Figure S5a). We also subtract the forced GMST response in the CMIP5 historical simulations from the GMST observations (Figure S5b). All of these methods consistently indicate a 0.11°-0.12°C standard deviation of internal GMST variability. Some observational data such as HadCRUT4 are spatially incomplete and blend surface air temperature and SST. This may slightly influence the estimated internal variability of GMST and therefore the data-model comparison [*Cowtan et al.*, 2015]. ENSO variability in the tropical Pacific contributes to GMST variability.

Climate sensitivity values in these models depend on representations of different feedback processes in the atmosphere. Different approaches have been used to estimate climate sensitivity in climate models [*Yoshimori et al.*, 2016]. CMIP5 used the approach of *Gregory et al.* [2004] to calculate effective climate sensitivity. The values range from 2.1°-4.7°C across the CMIP5 models (Table S2), therefore covering a large uncertainty space. As the Transient Climate Response values show a narrower spread across the CMIP5 models, we find that the use of effective climate sensitivity can enhance correlation analyses in this study.

3. Results

3.1. Observed Big Jump of Record Warm GMST over 2014-2016

The mean of the six GMST datasets indicates that the past three years (2014-2016) taken together broke the previous record warm year set in 2010 by a large amount of 0.24°C (0.22°-0.27°C, mean and range of the six datasets) (Figure 1). 2014 alone was a record-breaking year in five of the six datasets, with a difference from the previous record that is within the observational uncertainty range (Figure S1). However, the 3-year jump of 0.24°C represents a large change compared with GMST variability. Such events with similar or greater record-breaking magnitudes over consecutive record-breaking years (0.24°C+ events hereinafter) are highly unusual in the instrumental records (Figure 1) [*Mann et al.*, 2017]. Most of the record increase in GMST over the past three years occurred in 2015 and 2016 during a strong El Niño. 2015 and 2016 surpassed 2014 by 0.15°C (0.11°-0.19°C) and 0.21°C (0.18°-0.24°C), respectively. In 2015-2016, forecasts were published [*Peyser et al.*, 2016; *UK Met Office*, 2015] predicting this jump in GMST using either operational forecast systems [*Folland et al.*, 2013] or Pacific sea level anomalies along with a dynamical-statistical method [*Peyser et al.*, 2016]. The subsequent observations confirm these GMST predictions.

In three longer datasets (HadCRUT4, Berkeley and Cowtan&Way), the 1877-1878 GMST spike was the only other possible 0.24°C+ event in the instrumental period (Figure S1). This 19th century event was prior to large anthropogenic climate forcing and warming, but it is also associated with relatively large uncertainty. The large drop of GMST in the following year (1879) suggests that this GMST spike was likely caused by natural and transient processes, particularly a possible strong El Niño in the Pacific [*Aceituno et al.*, 2009]. By contrast, recent predictions of GMST based on operational systems suggest that 2017 will be among the warmest

years and the GMST, although unlikely to exceed the 2016 record, will remain at a high level after the 2014-2016 jump [*UK Met Office*, 2016].

3.2. Unusually Large Oceanic Heat Releases from WP/NWP during 2014-2015

The 2014-2016 GMST jump is a combined effect of the long-term increase in the atmospheric GHG concentration and the short-term strong El Niño in the Pacific Ocean. The warming associated with the El Niño should not be considered as purely natural variability because, in addition to warming the SSTs along the eastern equatorial Pacific, the El Niño also released excess heat sequestered into the subsurface layer (50-300 m) of the WP, especially the NWP east of the Philippines (Figures 2, 3 and S6). This heat had built up over the previous two decades (Figures 2a and S7), leading to rapid sea level rise in the WP (up to four times faster than the global mean) since the 1990s due to the dominant thermosteric effect (Figures 3c and S2) [*Griffies et al.*, 2014; *Peyser et al.*, 2016].

The linear trends of the observed upper 700 m OHC indicate a total heat accumulation of $3.5\text{-}4.5\times10^{22}$ J in the WP during 1993-2012 (Figure 3a). As shown in the low-pass filtered time series, the gradual buildup of ocean heat in the WP/NWP started from around 1993-1994 (Figure S7). The heat accumulation in the WP is an important component of global ocean heat uptake during the same period [*Gleckler et al.*, 2016]. Both internal variability and external forcing contributed to this unprecedented heat accumulation in the WP. On decadal/interdecadal time scales, the PDO or IPO is the dominant variability mode in the Pacific region that can influence OHC and GMST [*England et al.*, 2014; *Mantua et al.*, 1997; *Medhaug et al.*, 2017; *Meehl et al.*, 2016; *Nieves et al.*, 2015; *Steinman et al.*, 2015]. It should be noted that the mechanisms of the PDO/IPO are still under investigation about whether it is an intrinsic variability mode, a mixture of tropical and higher latitude phenomena [*Newman et al.*, 2016], or involves a forced

component [*Smith et al.*, 2016]. The regression of the upper 700 m OHC onto the observed PDO or IPO indices since the 1950s suggests that the transition of PDO/IPO to their negative phase during 1993-2012 had caused heat accumulation primarily centered in the southwestern tropical Pacific (Figures 2c, S4 and S6). By contrast, the buildup of excess ocean heat in the NWP east of the Philippines is mainly attributable to factors external to the Pacific, including GHG forcing and possible remote effects of other ocean basins (Figures 2d, 3d and S6) [*Luo et al.*, 2012; *McGregor et al.*, 2014].

As a good indicator of OHC, two long-term high-quality tide gauge data from the NWP confirm the unusual heat accumulation during 1993-2012 (Figure 3c). The relative sea level data at Kwajalein and Guam since 1950 are well correlated, suggesting common mechanisms. Sea level trends show a clear change during the 1990s at both locations. According to a clear linear trend, the total sea level rise over 1993-2012 was 194 and 186 mm at Kwajalein and Guam, respectively. The regression of the detrended tide gauge data onto the PDO index suggests that natural variability can explain 53 and 75 mm sea level rise at the two sites, respectively (Figure 3d and S8). Thus, other factors including GHG forcing and remote oceanic effects likely played a more important role in causing the rapid sea level rise in the NWP during 1993-2012 (Figures 3c and S2) [*Hamlington et al.*, 2014; *Han et al.*, 2014].

The excess subsurface ocean heat in the WP/NWP rapidly resurfaced and was then released to the atmosphere during 2014-2015 (Figures 2, 3 and S9). Here 2013 is used as the reference level for the heat release during 2014 and 2015. Compared to 2013, the WP OHC shows a significant drop by about $4.0\text{-}5.2\times10^{22}$ J in 2015 (Figure 3a), with the maximum heat release at the NWP (Figure 2b and S6). Our results indicate that in addition to the natural and normal amount of ocean heat release, the strong 2015/2016 El Niño also completely released the

ocean heat accumulated in the NWP during 1993-2012 (Figure 3d). The intense heat release resulted in a drastic sea level fall in the NWP by up to 300 mm during 2013-2015 (Figure S2). As a consequence, the once fastest sea level rise east of the Philippines as evidenced in altimetry data tends to subside after the 2014-2015 event (Figure S2).

EOF1 of the OHC in the tropical Pacific reveals an east-west seesaw pattern in the tropical Pacific (Figure S10). This seesaw also reflects vertical redistribution of ocean heat in the tropical Pacific associated with ENSO and PDO/IPO as well as induced by external forcing (Figure S9). Following a gradual decline during 1993-2012, PC1 shows a large jump during 2013-2015 exceeding the previous events associated with strong El Niño (Figure S10). It indicates an eastward movement and rapid upward emergence of massive ocean heat previously sequestered in deeper oceans (Figure S9), thereby directly boosting the Pacific SST and GMST (Figure 1).

During the large 1997-1998 El Niño, GMST also broke the previous record warm year set in 1995 by a large margin of 0.20°C (0.18°-0.22°C) (Figure 1). Conventional indices such as MEI and Niño3.4 suggest that the 1997-1998 El Niño was at least as strong as the 2015-2016 one (Figure S3). In terms of ocean heat release from the WP, and especially the NWP, however, the 2013-2015 event was clearly stronger and more pronounced than the previous ones during 1981-1982 and 1996-1997 (Figures 3 and S10). In fact, after two decades of unprecedented heat accumulation, the OHC in the WP dropped all the way back to the 1997 level in 2015. The ocean heat release started from 2014, coincident with the increase in GMST.

3.3. Model Simulations and Projections of Large Record-Breaking Events of GMST

The frequency, magnitude and duration of record-breaking events of GMST are important statistics for characterizing the risk of future extreme warming and other climate events. Next we use 40 CMIP5 models to examine these record-breaking event statistics in the 20th century simulations and 21st century projections. We first evaluate these statistics for each model before averaging them to generate the multi-model ensemble mean. In the historical runs of the CMIP5 models, the GMST records are usually broken by about 0°-0.2°C each time (Figure 4a). According to the multi-model ensemble average, a 0.24°C+ event such as observed in 2014-2016 is unlikely to have occurred under the 20th century external forcing alone; the average frequency of such an event is much less than one during the period 1901-2005, consistent with the observed lack of such an event during the 20th century (Figure 1).

In the context of the instrumental records of GMST, 13 (or 36%) of the 36 years from 1981-2016 were record-breaking years (Figure 1a). For the same period (1981-2016) of the CMIP5 model simulations and projections, the GMST records are broken by 10.5±2.6, 10.0±2.5, 9.9±2.3 and 10.2±2.5 (multi-model ensemble mean ± 1σ) times in the historical simulations (1981-2005) along with RCP2.6, RCP4.5, RCP6.0 and RCP8.5 projections (2006-2016), respectively. On centennial time scales, the record-breaking years account for 16%, 28%, 33% and 49% of the total of 95 years (2006-2100) given RCP2.6, RCP4.5, RCP6.0 and RCP8.5 emission scenarios, respectively (Figure S11).

The likelihood of the large 0.24°C+ events increases with the increase of GHG forcing. Over 2006-2100, the 0.24°C+ event occurs 0.7±0.7, 1.1±1.1, 2.1±1.7 and 6.0±2.7 times (multi-model ensemble mean ± 1σ) given RCP2.6, RCP4.5, RCP6.0 and RCP8.5 forcing, respectively (Figure 4a). The corresponding return periods are 136, 86, 45 and 16 years. In RCP8.5, the frequency of the 0.24°C+ event more than doubles after 2050. In addition to GHG forcing,

different effective climate sensitivity between the CMIP5 models (Table S2) is also a critical factor (Figure 4c). Under RCP8.5, for example, the 0.24°C+ event occurs 4.2 times over 2006-2100 given a low simulated climate sensitivity of 2.5°C. In contrast, a high climate sensitivity of 4.5°C can significantly increase the frequency to 9.3 times. These values are inevitably associated with uncertainty as shown by the scatter around the linear regression line in Figure 4c. Under the low RCP2.6 and RCP4.5 emission scenarios, climate sensitivity is less influential in modulating the frequency of the 0.24°C+ event. These distinct differences between different RCP projections highlight importance of present-day mitigation efforts in controlling the frequency and magnitude of future extreme GMST events.

Surprisingly, different internal variability of GMST in different models (Table S2) has a much weaker influence on the projected frequency of 0.24°C+ events in the 21st century, as shown by their low correlation (Figure 4d). Thus, the 0.24°C+ events in model projections are fundamentally modulated by GHG forcing and climate sensitivity, which jointly determine the overall upward slope of GMST (Figure S11). However, internal variability does influence the duration of the 0.24°C+ event. Stronger internal GMST variability tends to shorten the length of large record-breaking events of GMST and *vice versa* (Figure S12). This is because the cooling phases associated with large internal variability are more likely to compensate the GHG-induced warming and interrupt possible record-breaking streak of GMST. Given a 0.11°-0.12°C internal variability of the observed GMST (Figure S5), the 0.24°C+ event typically occurs over a course of 3.3-3.7 years (Figure S12), consistent with the observation during 2014-2016. In the historical simulations of the CMIP5 models, most record-breaking events are single-year events along with a couple of 2-year events (Figure 4b). The average frequency of 3-year and longer events is less

than one. During the 21st century, these long-lasting events occur 1.1±1.0, 2.2±1.5, 3.3±2.3 and 6.2±3.0 times on average in the RCP2.6, RCP4.5, RCP6.0 and RCP8.5 projections, respectively.

4. Discussion and Conclusions

The observed 0.24°C jump of record high GMST over three consecutive record-breaking years is highly unusual in the perspective of historical climate variability and change [*Mann et al.*, 2017]. It was mainly induced by a rapid release through the recent strong El Niño of the excess ocean heat previously accumulated in the NWP. According to model projections, large record-breaking events of GMST could become more routine by 2100, particularly if GHG emissions continue at high rates. Our analyses suggest that these large events, although often realized during El Niño, are fundamentally caused by the background warming due to GHG forcing. As caveats, we note that heat storage and rapid release from the WP/NWP may not be the only possible process that can cause 0.24°C+ events during the 21st century. Nonetheless, large GMST events similar to the observed 2014-2016 occur in the CMIP5 model projections both in terms of magnitude and mechanism (Figure S13).

Future large jumps in GMST will continue to be amplified in some regions, particularly over land areas and at high latitudes, and will continue to be associated with other climate extremes and impacts related to rapid warming. The increase in frequency, magnitude and duration of rapid global warming events has the potential to make adaptation more difficult. As shown by our RCP2.6 and RCP4.5 results, climate change mitigation would be effective at reducing or even eliminating such events in the long term.

References

Aceituno, P., M. del Rosario Prieto, M. E. Solari, A. Martínez, G. Poveda, and M. Falvey (2009), The 1877–1878 El Niño episode: associated impacts in south America, *Clim. Change*, *92*, 389-416.

Church, J. A., and N. J. White (2011), Sea-level rise from the late 19th to the early 21st century, *Surv. Geophys.*, *32*, 585-602.

Cowtan, K., and R. G. Way (2014), Coverage bias in the HadCRUT4 temperature series and its impact on recent temperature trends, *QJRMS*, *140*, 1935-1944.

Cowtan, K., Z. Hausfather, E. Hawkins, P. Jacobs, M. E. Mann, S. K. Miller, B. A. Steinman, M. B. Stolpe, and R. G. Way (2015), Robust comparison of climate models with observations using blended land air and ocean sea surface temperatures, *Geophys. Res. Lett.*, *42*, 6526-6534.

Ducet, N., P.-Y. Le Traon, and G. Reverdin (2000), Global high resolution mapping of ocean circulation from TOPEX/Poseidon and ERS-1 and -2, *J. Geophys. Res.*, *105*, 19477-19498.

England, M. H., S. McGregor, P. Spence, G. A. Meehl, A. Timmermann, W. Cai, A. S. Gupta, M. J. McPhaden, A. Purich, and A. Santoso (2014), Recent intensification of wind-driven circulation in the Pacific and the ongoing warming hiatus, *Nat. Clim. Change*, *4*, 222-227.

Flato, G., J. Marotzke, B. Abiodun, P. Braconnot, S. Chou, W. Collins, P. Cox, F. Driouech, S. Emori, and V. Eyring (2013), Evaluation of climate models, in *Climate Change 2013: The Physical Science Basis. Contribution of Working Group I to the Fifth Assessment Report of the Intergovernmental Panel on Climate Change*, edited, pp. 741-866, Cambridge University Press.

Folland, C. K., A. W. Colman, D. M. Smith, O. Boucher, D. E. Parker, and J. P. Vernier (2013), High predictive skill of global surface temperature a year ahead, *Geophys. Res. Lett.*, *40*, 761-767.

Gleckler, P. J., P. J. Durack, R. J. Stouffer, G. C. Johnson, and C. E. Forest (2016), Industrial-era global ocean heat uptake doubles in recent decades, *Nat. Clim. Change*, *6*, 394-398.

Gregory, J., W. Ingram, M. Palmer, G. Jones, P. Stott, R. Thorpe, J. Lowe, T. Johns, and K. Williams (2004), A new method for diagnosing radiative forcing and climate sensitivity, *Geophys. Res. Lett.*, *31*, L03205.

Griffies, S. M., et al. (2014), An assessment of global and regional sea level for years 1993-2007 in a suite of interannual CORE-II simulations, *Ocean Model.*, *78*, 35-89.

Hamlington, B., M. Strassburg, R. Leben, W. Han, R. Nerem, and K. Kim (2014), Uncovering an anthropogenic sea-level rise signal in the Pacific Ocean, *Nat. Clim. Change*, *4*, 782-785.

Han, W., G. A. Meehl, A. Hu, M. A. Alexander, T. Yamagata, D. Yuan, M. Ishii, P. Pegion, J. Zheng, and B. D. Hamlington (2014), Intensification of decadal and multi-decadal sea level variability in the western tropical Pacific during recent decades, *Clim. Dyn.*, *43*, 1357-1379.

Hansen, J., R. Ruedy, M. Sato, and K. Lo (2010), Global surface temperature change, *Rev. Geophys.*, *48*, RG4004.

Herring, S., A. Hoell, M. P. Hoerling, J. P. Kossin, C. J. Schreck III, and P. A. Stott (2016), Explaining extreme events of 2015 from a climate perspective, *Bull. Am. Meteorol. Soc.*, *97*, S1-S145.

Herring, S., N. Christidis, A. Hoell, J. Kossin, C. J. Schreck III, and P. A. Stott (2018), Explaining extreme events of 2016 from a climate perspective, *Bull. Am. Meteorol. Soc.*, *99*, S1-S157.

296 Holgate, S. J., A. Matthews, P. L. Woodworth, L. J. Rickards, M. E. Tamisiea, E. Bradshaw, P.
297 R. Foden, K. M. Gordon, S. Jevrejeva, and J. Pugh (2013), New Data Systems and Products
298 at the Permanent Service for Mean Sea Level, *J. Coast. Res.*, *29*, 493-504.
299 Hu, S., and A. V. Fedorov (2016), Exceptionally strong easterly wind burst stalling El Niño of
300 2014, *Proc. Natl. Acad. Sci. U. S. A.*, *113*, 2005-2010.
301 Ishihara, K. (2006), Calculation of global surface temperature anomalies with COBE-SST,
302 *Weather Serv. Bull.*, *73*, S19-S25.
303 Ishii, M., and M. Kimoto (2009), Reevaluation of historical ocean heat content variations with
304 time-varying XBT and MBT depth bias corrections, *J. Oceanogr.*, *65*, 287-299.
305 Levitus, S., et al. (2012), World ocean heat content and thermosteric sea level change (0-2000 m),
306 1955-2010, *Geophys. Res. Lett.*, *39*, L10603.
307 Luo, J.-J., W. Sasaki, and Y. Masumoto (2012), Indian Ocean warming modulates Pacific
308 climate change, *Proc. Natl. Acad. Sci. U. S. A.*, *109*, 18701-18706.
309 Mann, M. E., S. K. Miller, S. Rahmstorf, B. A. Steinman, and M. Tingley (2017), Record
310 temperature streak bears anthropogenic fingerprint, *Geophys. Res. Lett.*, *44*, 7936-7944.
311 Mantua, N. J., S. R. Hare, Y. Zhang, J. M. Wallace, and R. C. Francis (1997), A Pacific
312 interdecadal climate oscillation with impacts on salmon production, *Bull. Am. Meteorol.*
313 *Soc.*, *78*, 1069-1079.
314 McGregor, S., A. Timmermann, M. F. Stuecker, M. H. England, M. Merrifield, F.-F. Jin, and Y.
315 Chikamoto (2014), Recent Walker circulation strengthening and Pacific cooling amplified
316 by Atlantic warming, *Nat. Clim. Change*, *4*, 888-892.
317 Medhaug, I., M. B. Stolpe, E. M. Fischer, and R. Knutti (2017), Reconciling controversies about
318 the 'global warming hiatus', *Nature*, *545*, 41-47.

Meehl, G. A., A. Hu, B. D. Santer, and S.-P. Xie (2016), Contribution of the Interdecadal Pacific Oscillation to twentieth-century global surface temperature trends, *Nat. Clim. Change*, *6*, 1005-1008.

Morice, C. P., J. J. Kennedy, N. A. Rayner, and P. D. Jones (2012), Quantifying uncertainties in global and regional temperature change using an ensemble of observational estimates: The HadCRUT4 data set, *J. Geophys. Res.*, *117*, D08101.

Newman, M., M. A. Alexander, T. R. Ault, K. M. Cobb, C. Deser, E. Di Lorenzo, N. J. Mantua, A. J. Miller, S. Minobe, and H. Nakamura (2016), The Pacific decadal oscillation, revisited, *J. Clim.*, *29*, 4399-4427.

Nicolas, J. P., A. M. Vogelmann, R. C. Scott, A. B. Wilson, M. P. Cadeddu, D. H. Bromwich, J. Verlinde, D. Lubin, L. M. Russell, and C. Jenkinson (2017), January 2016 extensive summer melt in West Antarctica favoured by strong El Niño, *Nat. Commun.*, *8*, 15799(2017).

Nieves, V., J. K. Willis, and W. C. Patzert (2015), Recent hiatus caused by decadal shift in Indo-Pacific heating, *Science*, *349*, 532-535.

NOAA (2015), NOAA declares third ever global coral bleaching event, http://www.noaanews.noaa.gov/stories2015/100815-noaa-declares-third-ever-global-coral-bleaching-event.html.

Paris Agreements (2015), Adoption of the Paris Agreement FCCC/CP/2015/L.9/Rev.1, United Nations Framework Convention on Climate Change, 2015.

Peyser, C. E., J. Yin, F. W. Landerer, and J. E. Cole (2016), Pacific sea level rise patterns and global surface temperature variability, *Geophys. Res. Lett.*, *43*, 8662-8669.

Rayner, N., D. E. Parker, E. Horton, C. Folland, L. Alexander, D. Rowell, E. Kent, and A. Kaplan (2003), Global analyses of sea surface temperature, sea ice, and night marine air temperature since the late nineteenth century, *J. Geophys. Res.*, *108*, 4407.

Roemmich, D., and J. Gilson (2009), The 2004-2008 mean and annual cycle of temperature, salinity, and steric height in the global ocean from the Argo Program, *Prog. Oceanogr.*, *82*, 81-100.

Rohde, R., R. Muller, R. Jacobsen, S. Perlmutter, A. Rosenfeld, J. Wurtele, J. Curry, C. Wickhams, and S. Mosher (2013), Berkeley Earth Temperature Averaging Process, *Geoinfor. Geostat.: An Overview*, *13*, 20-100.

Simpkins, G. (2017), Snapshot: Extreme Arctic heat, *Nat. Clim. Change*, *7*, 95-95.

Smith, D. M., B. B. Booth, N. J. Dunstone, R. Eade, L. Hermanson, G. S. Jones, A. A. Scaife, K. L. Sheen, and V. Thompson (2016), Role of volcanic and anthropogenic aerosols in the recent global surface warming slowdown, *Nat. Clim. Change*, *6*, 936–940.

Steinman, B. A., M. E. Mann, and S. K. Miller (2015), Atlantic and Pacific multidecadal oscillations and Northern Hemisphere temperatures, *Science*, *347*, 988-991.

Taylor, K. E., R. J. Stouffer, and G. A. Meehl (2012), An overview of CMIP5 and the experiment design, *Bull. Am. Meteorol. Soc.*, *93*, 485-498.

UK Met Office (2015), Forecast expects 2016 to be among the warmest years, http://www.metoffice.gov.uk/news/releases/2015/global-temperature.

UK Met Office (2016), 2017: another very warm year for global temperatures, http://www.metoffice.gov.uk/news/releases/2016/global-forecast-2017.

Vose, R. S., D. Arndt, V. F. Banzon, D. R. Easterling, B. Gleason, B. Huang, E. Kearns, J. H. Lawrimore, M. J. Menne, and T. C. Peterson (2012), NOAA's merged land–ocean surface temperature analysis, *Bull. Am. Meteorol. Soc.*, *93*, 1677-1685.

Wolter, K., and M. S. Timlin (2011), El Niño/Southern Oscillation behaviour since 1871 as diagnosed in an extended multivariate ENSO index (MEI. ext), *Intl. J. Climatology*, *31*, 1074-1087.

Wu, Z. H., N. E. Huang, J. M. Wallace, B. V. Smoliak, and X. Y. Chen (2011), On the time-varying trend in global-mean surface temperature, *Clim. Dyn.*, *37*, 759-773.

Yoshimori, M., M. Watanabe, H. Shiogama, A. Oka, A. Abe-Ouchi, R. Ohgaito, and Y. Kamae (2016), A review of progress towards understanding the transient global mean surface temperature response to radiative perturbation, *Progress in Earth and Planetary Science*, *3*, 1-14.

Acknowledgements

The authors thank many observation, modeling, data service and climate research centers for making their data and scripts available. We appreciate the comments from the anonymous reviewers. Part of the work was done during JY's sabbatical at Princeton University and GFDL/NOAA. JY thanks the GFDL host S. Griffies and the Visiting Scientist Program of Princeton University. The research was supported by NOAA grant #NA13OAR4310128 and NSF grants #1304083 and #1513411. The observational and model data used in this study can be accessed from the URLs found in the tables. For all other data inquiries, please contact Jianjun Yin (yin@email.arizona.edu).

Figure Captions

Figure 1. Observed GMST anomalies and record-breaking events. (a) Time series of six GMST datasets and the mean of the six datasets. (b) Cumulative record-breaking magnitude of GMST during consecutive record-breaking years after 1980 (mean and range of the six datasets). For the 2014-2016 event, the cumulative record-breaking magnitude of GMST is the difference between 2016 and 2010 (the previous record prior to the event). All anomaly values are relative to the 1981-2010 period. The mean in (a) is calculated for the common period of the six datasets (1891-2016). Red dots denote record-breaking years of GMST after 1980. See Figure S1 for plots of each dataset and associated uncertainty.

Figure 2. Interdecadal accumulation and rapid release of ocean heat in the upper 700 m (10^{18} J, Levitus data). (a) Total heat accumulation during 1993-2012 based on the linear trend. (b) Ocean heat release (negative values) during 2013-2015. Notice the different scale. (c) 1993-2012 ocean heat accumulation due to the transition of PDO/IPO to their negative phase. (d) Difference between (a) and (c) indicating the ocean heat accumulation due to factors external to the Pacific. The green boxes in (a), (c) and (d) indicate WP (120°E-180°E, 20°S-20°N), SWP (145°E-195°E, 0°-15°S) and NWP (120°E-180°E, 3°N-18°N), respectively. The circles mark Kwajalein and Guam (Figure 3c). See Figure S6 for similar analysis with the Ishii data.

Figure 3. Consistent changes of observed ocean temperature, heat content and sea level in the WP and NWP. (a) Time series of the upper 700 m OHC anomalies in the WP from three datasets. The dashed lines indicate 20-year linear trends prior to the 1981-1982, 1996-1997 and 2013-2015 ocean heat release events associated with strong El Niño. (b) Anomalies of the area mean ocean temperatures in the WP as a function of depth and time (Levitus data). The vertical dashed lines indicate the 1981-1982, 1996-1997 and 2013-2015 ocean heat releases from the subsurface

layer (horizontal dashed lines). (c) Two long-term high-quality tide gauge data of relative sea level at Kwajalein and Guam in the NWP. The dashed lines show the linear trend during 1950-1992 and 1993-2012. The reconstructed global mean sea level rise is also plotted with uncertainty. (d) 1993-2012 ocean heat accumulation in the NWP (based on the linear trend) and the contributions from PDO (Figure S8) and other factors external to the Pacific (total minus PDO), and the magnitudes of the large drops during 2013-2015 and 1996-1997. The tide gauge data at Kwajalein and Guam are analyzed similarly.

Figure 4. Statistics of record-breaking events of GMST in the CMIP5 model simulations and projections. (a) and (b) Histogram of the cumulative magnitude (a) and duration (b) of record-breaking events. (c) and (d) Frequency of the 0.24°C+ events over 2006-2100 as a function of GHG forcing and effective climate sensitivity (c), and internal variability of GMST (d). The record-breaking events are counted from 1901-2005 in the historical simulations and from 2006-2100 in the RCP projections. The frequency indicates multi-model ensemble mean (± 1σ) of the occurrence times during the entire period. The numbers in the legend denote the model ensemble size. One realization is used for each run and each model. Note 0.24°C as the divide for the 0.2°-0.24°C and 0.24°-0.3°C intervals in (a). In (c) and (d), each dot indicates one model result. The lines are the linear fits to the data with correlation. Internal variability of GMST is estimated using 200-year piControl simulations of the CMIP5 models (Table S2).

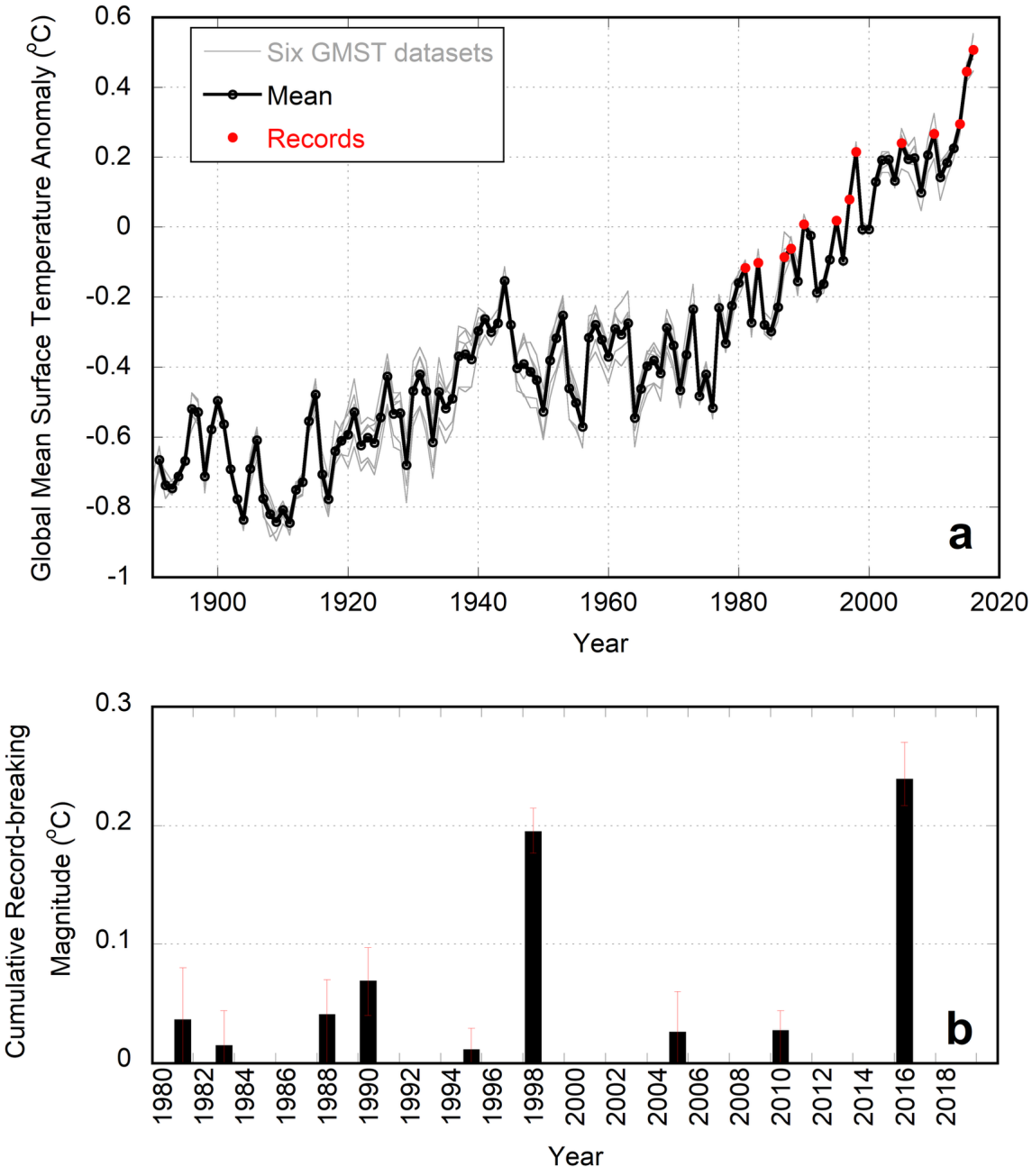

2017GL076500-f01-z-.tif

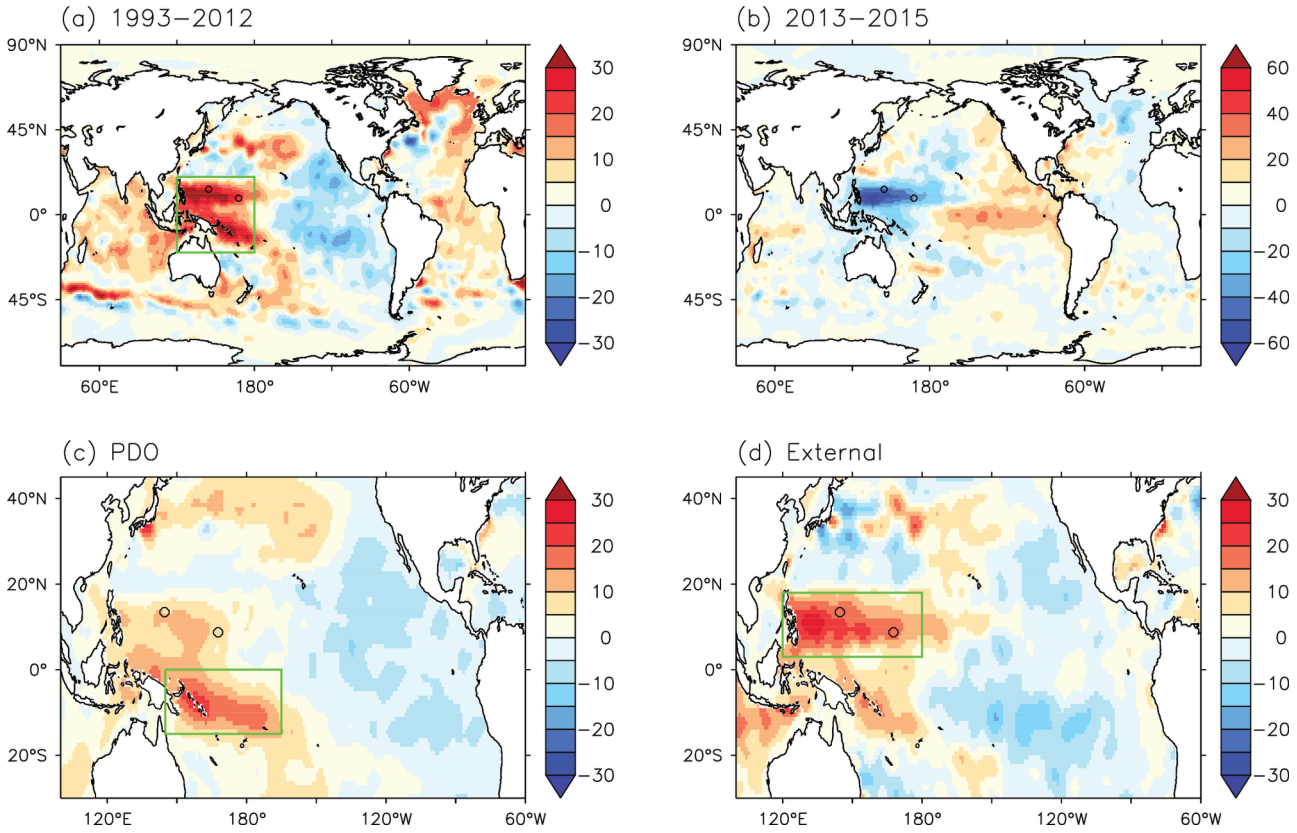

2017gl076500-f02-z-.eps

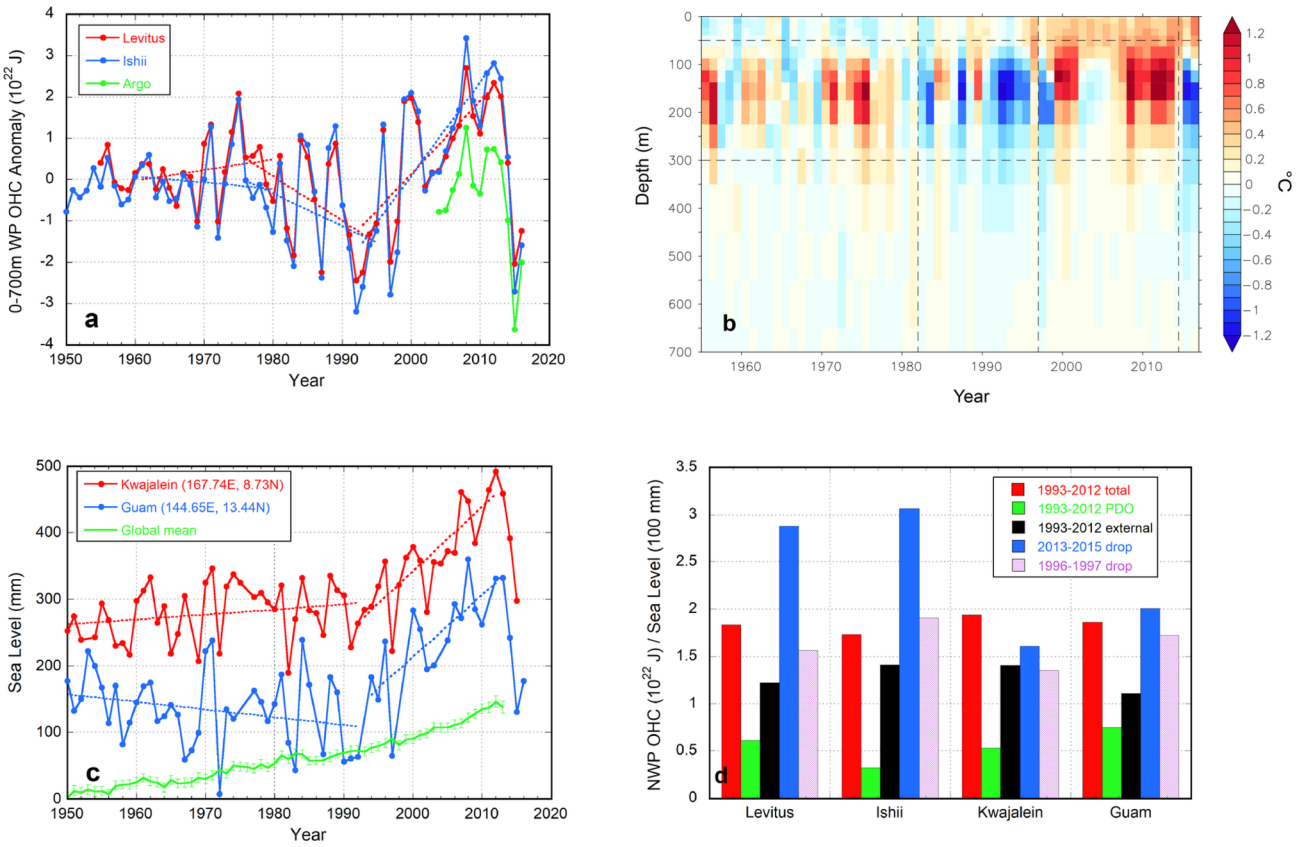

2017GL076500-f03-z-.tif

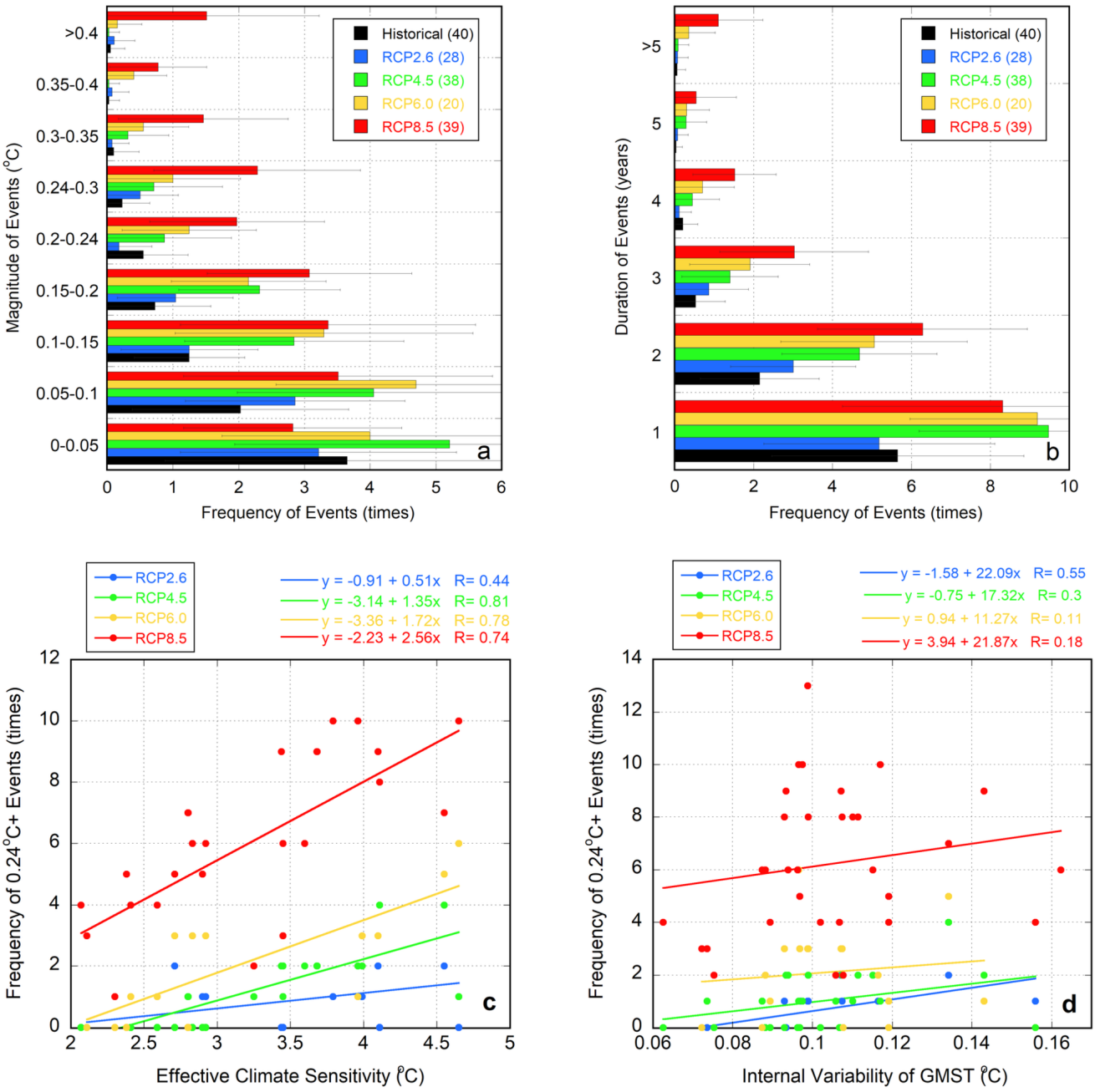

2017GL076500-f04-z-.tif

Table 1. Observational datasets used in the present study.

	Dataset	Institute	Period	Reference	Website
GMST	HadCRUT4	UK Met Office Hadley Centre	1850-2016	*Morice et al.*, 2012	http://www.metoffice.gov.uk/hadobs/hadcrut4/data
	GISTEMP	NASA GISS	1880-2016	*Hansen et al.*, 2010	http://data.giss.nasa.gov/gistemp/
	NOAAGlobalTemp	NOAA NCEI	1880-2016	*Vose et al.*, 2012	https://www.ncdc.noaa.gov/data-access/marineocean-data/noaa-global-surface-temperature-noaaglobaltemp
	JMA	Japanese Meteorol. Agency	1891-2016	*Ishihara*, 2006	http://ds.data.jma.go.jp/tcc/tcc/products/gwp/temp/ann_wld.html
	Berkeley	Berkeley Earth	1850-2016	*Rohde et al.*, 2013	http://berkeleyearth.org/
	Cowtan&Way	University of York	1850-2016	*Cowtan and Way*, 2014	http://www-users.york.ac.uk/~kdc3/papers/coverage2013/series.html
OHC	Levitus	NOAA NCEI	1955-2016	*Levitus et al.*, 2012	https://www.nodc.noaa.gov/OC5/3M_HEAT_CONTENT/
	Ishii	Japanese Meteorol. Agency	1950-2016	*Ishii and Kimoto*, 2009	http://www.data.jma.go.jp/gmd/kaiyou/english/ohc/ohc_data_en.html
	Argo	International Argo Program	2004-2016	*Roemmich and Gilson*, 2009	http://www.argo.ucsd.edu
Sea Level	Tide gauge	PSMSL	1950-2015 1948-2016	*Holgate et al.*, 2013	http://www.psmsl.org/data/obtaining
	Altimetry	AVISO	1993-2016	*Ducet et al.*, 2000	http://www.aviso.altimetry.fr/en/data/data-access.html
	Global mean Reconstruction	CSIRO	1880-2013	*Church and White*, 2011	http://www.cmar.csiro.au/sealevel/sl_data_cmar.html
ENSO	MEI	NOAA ESRL	1950-2016	*Wolter and Timlin*, 2011	https://www.esrl.noaa.gov/psd/enso/mei/
	Niño3.4	NOAA ESRL	1870-2016	*Rayner et al.*, 2003	https://www.esrl.noaa.gov/psd/gcos_wgsp/Timeseries/Nino34/
PDO	PDO	NOAA NCEI	1854-2016	*Mantua et al.*, 1997	https://www.ncdc.noaa.gov/teleconnections/pdo/